Measurements Based mmW Channel Modelling in Railway Environments

Nicholas Attwood, François Gallée, Patrice Pajusco, Marion Berbineau

Measurements Based mmW Channel Modelling in Railway Environments

Nicholas ATTWOOD*, François GALLEE*, Patrice PAJUSCO*, Marion BERBINEAU†
*IMT-Atlantique - Lab-STICC, Brest, France, [nicholas.attwood, francois.gallee, patrice.pajusco]@imt-atlantique.fr
†Université Gustave Eiffel, COSYS-LEOST, Lille, France, marion.berbineau@univ-eiffel.fr

***Abstract*—This paper presents results from radio propagation channel characterization for a platooning scenario in a railway environment. The measurements were conducted using the IMT Atlantique / Lab-STICC SIMO CS system, operating at a carrier frequency of 60 GHz with a bandwidth of 180 MHz. The measurement site is a marshalling yard within a railway trial center. Based on these measurements, the Path Loss in a LoS situation is analyzed, along with the evolution of the RMS delay spread. The results are compared to those from a previous measurement campaign conducted on a similar track at mmWave frequencies. Finally, the parameters of the Rician distribution used to model small-scale fading are presented.**

***Index Terms*—channel sounder, mmWave, antennas, propagation, measurements, railway, platooning.**

I. Introduction

The global transportation system is entering the era of full automation, and railway transportation is no exception. In Europe, railway communication systems are undergoing a significant transformation with the development of the FRMCS. This evolution is also evident in France, where the outdated GSM-R communication system will be upgraded to comply with 5G. The new communication standard brings enhanced features and possibilities, such as improved passenger entertainment through higher data rates on trains, as well as enabling autonomous operation scenarios. The first autonomous scenario involves remotely controlling a train from the garage to a train station. The second scenario, known as platooning, refers to the virtual coupling of two trains following the same track. Achieving these scenarios requires meeting specific requirements. The first is the need for high data rates to ensure safety on high-speed tracks and enhance onboard entertainment. The second requirement is reliability. Indeed, since trains operate at varying speeds — which can be very high, such as a maximum of 320 km/h on dedicated lines in France — and have long braking distances, the system must be reliable enough to maintain a communication link. The main limitation arises from the available bands for these new scenarios. Although FRMCS uses 3G, 4G, and 5G technologies, the available bands and bandwidth remain limited. Therefore, it is essential to explore new frequency bands, with the millimeter-wave band being a promising candidate for such applications. In particular, the 60 GHz band is unlicensed in France, allowing for several gigahertz of bandwidth with low latency. Nonetheless, radio propagation at this frequency in the railway environment is very challenging. In the literature, only a few papers [1], [2], [3], [4], [5], [6] present results from measurement campaigns, and only [7] provides results at 60 GHz. To address this gap, a collaborative project was initiated, and results from a measurement campaign conducted in a railway environment will be presented. The paper is organized as follows: the first section introduces the SDR-based channel sounder developed at IMT Atlantique for channel measurements. The second section describes the railway environment used for the measurements. Finally, the last section presents the main statistical parameters, including path loss evolution, RMS delay spread, and small-scale fading, along with a comparison to similar measurements at 28 GHz presented in [6].

II. The IMT-Atlantique's SIMO Channel Sounder at 60 GHz

At IMT Atlantique/Lab-STICC, a Channel Sounder (CS) has been developed to operate in the V-Band and especially at 60 GHz, with Single Input Multiple Output (SIMO) capabilities [8]. The architecture of the CS enables dynamic measurements in various complex environments. It is built around a commercial demonstration board developed by Analog Devices for the up- and down-conversion of the baseband transmitted signal, combined with a Software-Defined Radio (SDR) platform to digitize the received sounding sequence. In this setup, the selected SDR platform is the USRP X310 [9]. Fig 1 shows the complete integration of the transmitter (Tx) and the receiver (Rx) components. Each part of the CS is synchronized using an independent Rubidium clock, which is further synchronized with Global Navigation Satellite System (GNSS) data. Furthermore, the Tx component is the moving element and includes additional features, such as a Real-Time Kinematic (RTK) module to improve localization accuracy and a fisheye camera, with accurate time stamp, used to capture images of the immediate surroundings during the measurement. The key specifications are outlined in Tab. I.

III. Measurement Environment and Scenario

The Railway Trial Center (CEF) in Valenciennes was used to perform dynamic measurements in a real, controllable environment. The CEF is divided into different areas, each used to conduct various tests on new trains, such as endurance and braking tests. Additionally, there is an area where the train remains stationary, and tests are conducted on it. This setup allows for the repetition of different scenarios in identical

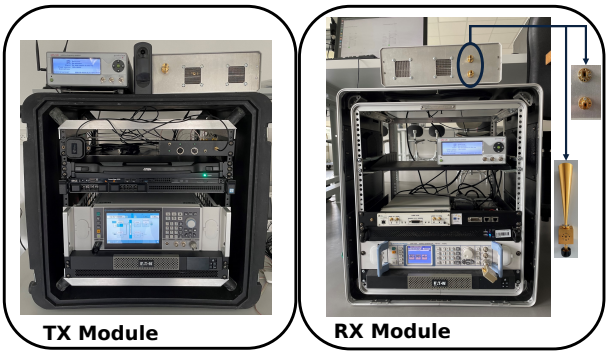

Fig. 1. Picture of the Tx and the Rx unit.

TABLE I
MAIN CHARACTERISTICS OF THE CHANNEL SOUNDER

Type	Value
Center Frequency	57 - 60 GHz
Bandwidth	180 MHz
Maximum Excess Delay	2 µs
Rx Antenna	10 dBi horn antenna
Tx Antenna	5 dBi horn antenna
Polarization	Vertical, Horizontal, and Dual V/H

surroundings, as the static tests are conducted throughout the day. Fig. 2 shows a aerial view of the static area available for our measurements. As shown in Fig. 2, there are three distinct tracks. The track labeled **VES1** is primarily composed of concrete, while **VES2** and **VES3** have a more traditional design, featuring ballast, iron rails, and wooden sleepers. Moreover, between tracks **VES1** and **VES2**, there is a catenary line supported by a series of aligned catenary masts, which represents a typical electrified railway. Track **VES3** does not have this catenary mast line but instead features lampposts, which are smaller than the catenary masts but are also regularly spaced.

Fig. 2. Map of the CEF.

In this environment, several scenarios have been investigated. The first scenario is similar to the one proposed by 3GPP [10]. In this scenario, 3GPP suggests installing Remote Radio Heads (RRH) regularly spaced along the track, controlled by different Baseband Units (BBU). The second scenario investigated is platooning. As mentioned earlier, the platooning maneuver involves creating a virtual coupling between two trains. The goal is to maintain a relatively short distance between the trains, from few meters to several hundreds of meters, by establishing a communication link. In the scope of this paper, this scenario is the one retained and took place on track **VES2**. As mentioned earlier, this track represents a typical electrified railway and has a maximum length of 150 m, limited by the environment. In [7], the authors proposed installing the communication system on the coupling mechanism of the train. To set up a similar installation, a rail trolley is used to position the Tx, while the Rx is installed at the beginning of the track. Fig. 3 shows the installation of the CS. It can be noted that both components are installed at a height of 80 cm, which is the standard height of the coupling system on the train.

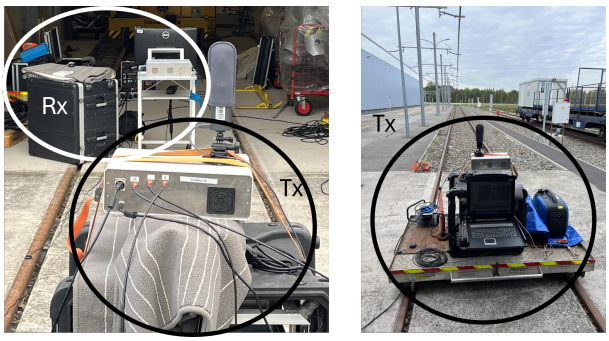

Fig. 3. Installation of the Rx and Tx in the environment.

In this configuration, 12 measurements were taken, resulting in 50 GB of data, composed by Tx moving back and to the Rx. Each measurement provide the complex channel transfer function, with a spatial step of $\lambda/10$. The next section presents the different statistical parameters and the results for all the measurements.

IV. Experimental Results

A. Visibility Situation

Before introducing the different statistical parameters, it is necessary to classify the visibility of the measurements. In this scenario, there are three possibilities: the first is Line-of-Sight (LoS), where the Tx and Rx are completely aligned, as they are on the same track. Next, there is a slight curve, leading to Obstructed Line-of-Sight (OLoS) due to the alignment of the catenary masts, which block the optical link. Finally, the curve of the track results in Non-Line-of-Sight (NLoS) due to a metallic warehouse blocking the optical link.

To distinguish between the different cases, a geometric technique based on triangles is used. The idea is to have two points around a catenary mast, for example. The distance between each point and the mast is determined by the length of the mast, and the configuration is arranged to be parallel to the track. These points, along with the position of the Rx, form a triangle. If the Tx position lies within the area formed by this triangle, it is considered NLoS; otherwise, the position is considered LoS.

Fig. 4. The different visibility situation during the measurement.

B. Large Scale Fading

The first parameter extracted from the measurement data is the Path Loss (PL). In this case, the single-slope PL model is considered, and its definition is presented in Eq. 1, where α represents the Path Loss Exponent (PLE) and X_{σ}^{mod} represents the shadowing. The shadowing is modeled using a log normal distribution, with σ as the standard deviation. The PL is obtained by averaging the received power over a stationary area. In our case, the stationary area has a size of 40λ. The stationary area size has been characterized, using the correlation on the Power Delay Profile (PDP).

$$PL[dB] = 10\alpha \log_{10}(d) + X_{\sigma}^{\text{mod}} \quad (1)$$

The technique for obtaining the Path Loss Exponent (PLE) is divided into two steps. The first step is to reduce the impact of the noise on the PL estimation. To do this, the PL from the measurement is divided into equal intervals. For each interval, the median value is computed. Once the medians are obtained, only the intervals where the median is higher than the noise floor are retained. An example is shown in Fig. 5, where the green line represents the visibility case. The discontinuities in this green line indicate the presence of NLoS situations. In this specific scenario, the NLoS situation is not taking into account because there are below the noise threshold.

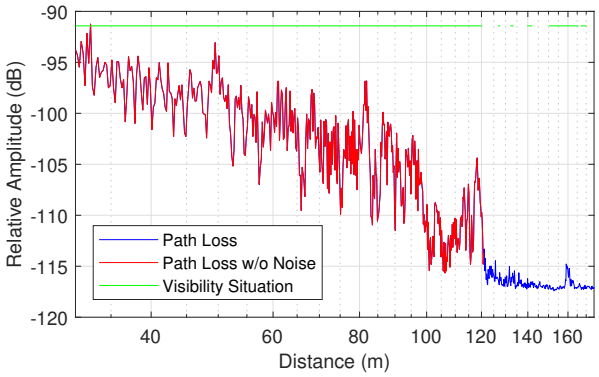

Fig. 5. PL and interval technique for the first Rx.

Then, for each receiver, a second step is applied, which involves performing a linear regression for each visibility condition, and the Path Loss Exponent (PLE) is obtained. Fig. 6 shows the result obtained for the LoS visibility condition. As seen in Fig. 5, the majority of the measurements are in LoS conditions. Furthermore, Fig. 6 shows values of 2.91 and 3.02 for the PLE for Rx1 and Rx2, respectively. Tab. II presents the results obtained for all the measurements. It can be noted that the PLE for both polarizations are very close to each other, with a mean value greater than 2, and can be compared to the results proposed in [6]. In that study, the author proposed a PL model based on a single-slope model extracted from measurements taken in a marshalling yard. The PLE proposed was 2.27 for an omni-directional, vertically polarized antenna. In our case, the obtained mean PLE is 2.76. This result shows that the 60 GHz radio propagation channel incurs additional losses, such as those due to oxygen absorption, for example, which impact the PLE by adding 0.3.

TABLE II
PLE OBTAIN FOR ALL THE MEASUREMENTS IN LOS.

Polarization	Rx No	Min	Max	Mean	Std
Horizontal	Rx1	2.73	2.93	2.80	0.11
	Rx2	2.80	3.07	2.90	0.15
Vertical	Rx1	2.45	3.11	2.76	0.33
	Rx2	2.4	3.08	2.76	0.34

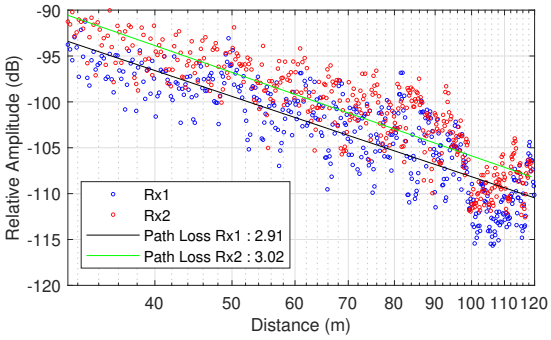

Fig. 6. PLE for the two Rx from the measurement, for horizontal polarization.

Once the PLE is obtained from the measurement, the computation to obtain the shadowing value is performed. The shadowing represents the variation around the single-slope model. This variation is modeled with a random variable following a normal distribution, with σ as its standard deviation. The parameter σ is obtained using Maximum Likelihood Estimation (MLE), and the results for both Rx are presented in Fig. 7. From these measurements, it can be seen that the σ parameter equals 3.03 and 2.7 dB for the first and second Rx, respectively.

Tab. III presents the results obtained from all the measurements for the LoS visibility condition. From these results, it can be noted that the polarization does not significantly impact the shadowing factor. From the measurements made in [6], the shadowing factor is 2.8 dB, which is close to the result obtained from our measurement campaign.

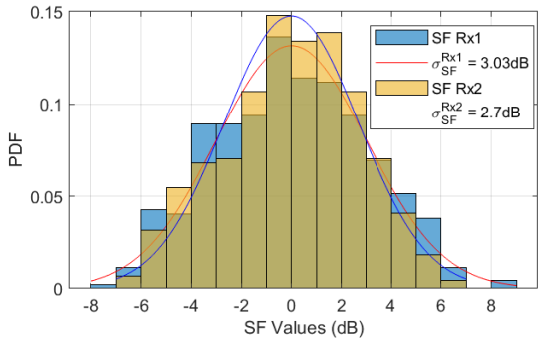

Fig. 7. Shadowing factor for both Rx from the measurement made on **VES2**.

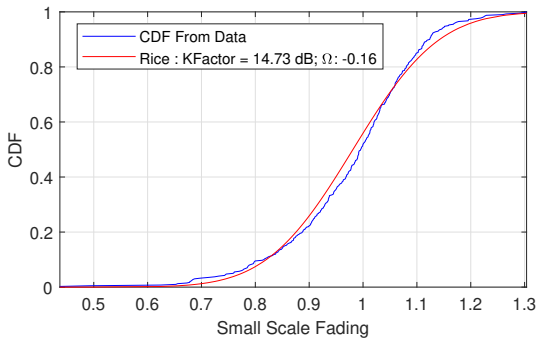

Fig. 8. CDF.

TABLE III
SHADOWING FACTOR OBTAIN FOR ALL THE MEASUREMENTS IN LOS.

Polarization	Rx No	Min	Max	Mean	Std
Horizontal	Rx1	2.94	3.01	2.98	0.04
	Rx2	2.61	2.67	2.64	0.03
Vertical	Rx1	2.67	2.94	2.79	0.14
	Rx2	2.54	2.88	2.67	0.18

TABLE IV
RICIAN PARAMETERS OBTAIN FOR ALL THE MEASUREMENTS IN LOS.

Parameter	Polar.	Rx No	Min	Max	Mean	Std
K[dB]	H	Rx1	14.64	14.66	14.65	0.01
		Rx2	14.52	14.64	14.60	0.07
	V	Rx1	14.74	16.14	15.41	0.70
		Rx2	14.79	16.15	15.53	0.69
Ω[dB]	H	Rx1	-0.19	-0.19	-0.19	0.00
		Rx2	-0.19	-0.18	-0.18	0.01
	V	Rx1	-0.19	-0.15	-0.17	0.02
		Rx2	-0.19	-0.16	-0.17	0.02

C. Small Scale Fading

The small-scale fading models the power fluctuations due to the presence of Multi-Path Components (MPCs) within a stationary area. In our case, small-scale fading is obtained using the same method presented for the Path Loss (PL) extraction, with the only difference being that only the intervals where the median value exceeds the noise floor are retained. Several random distributions exist in the literature to model these fluctuations. In this paper, only the Rician distribution is used to model these power variations. The Probability Density Function (PDF) of the Rician distribution is presented in Eq. 2, where K represents the ratio of the power contributions from the LoS to the remaining MPCs, Ω is defined as the total power received from all paths, and I_0 is the modified Bessel function of the first kind with order 0.

$$f(x|K,\Omega) = \frac{2(K+1)x}{\Omega} \exp\left(-K - \frac{(K+1)r^2}{\Omega}\right) I_0\left(2r\sqrt{\frac{K(K+1)}{\Omega}}\right) \quad (2)$$

The small-scale distribution parameters are computed within a stationary area, and an example of the results is shown in Fig. 8 for the first Rx under LoS visibility conditions. In this stationary area window, the K factor is 14.73 dB for the first Rx, and the parameter Ω is -0.16 dB. This value of the K factor indicates a strong main component with additional MPCs, but with lower power contributions. Then, the parameters are extracted for all the measurements, and the mean value for each parameter is retained.

Finally, Tab. IV shows the K-Factor and Ω parameters obtained for the small-scale fading. The results show that the vertical polarization has a higher K-Factor than the horizontal polarization. This can be explained by the impact of the environment. Indeed, in the railway environment, the catenary mast lines are vertical and interact more effectively with a vertically polarized wave, leading to higher MPCs near the main path. Due to the limited bandwidth of the CS, these additional MPCs are included within the main path.

D. PDP and RMS Delay Spread

Once the large-scale parameters are obtained, the focus can shift to the temporal dispersion of the MPCs. The main parameter used to describe this dispersion is the RMS delay spread, which is defined in Eq. 3, where $\overline{\tau} = \frac{\sum_{i=0}^{N} \tau_i P(x_k,\tau_i)}{\sum_{i=0}^{N} P(x_k,\tau_i)}$ represents the mean delay, and $P(x_k,\tau)$ is the Power Delay Profile (PDP) at the distance x_i.

$$D_s = \sqrt{\frac{\sum_{i=0}^{N}(\tau_i - \overline{\tau})^2 P(x_k,\tau_i)}{\sum_{i=0}^{N} P(x_k,\tau_i)}} \quad (3)$$

The computation to obtain the RMS delay spread involves two steps. The first step is to remove the noise from the PDP. The second step is divided into two parts: first, a threshold of 30 dB is applied, and PDPs with dynamics lower than 20 dB are excluded from the computation. An example of the computed results is presented in Fig. 9 for both Rx in LoS conditions. From this result, it can be seen that at 100 m, the RMS delay spread increases, reaching its maximum value. This increase is due to the presence of the catenary

TABLE V
LOG RMS DELAY SPREAD OBTAIN FOR ALL THE MEASUREMENTS IN LOS.

Polarization	Rx No	Min	Max	Mean	Std
Horizontal	Rx1	-8.41	-8.41	-8.41	0.00
	Rx2	-8.44	-8.43	-8.44	0.01
Vertical	Rx1	-8.46	-8.40	-8.43	0.03
	Rx2	-8.47	-8.40	-8.44	0.04

mast lines, which partially block the optical link but not completely, thus still being considered LoS. This alignment can also be observed in Fig. 5, where at 100 m, the received power decreases, but the number of MPCs increases due to additional diffraction from the catenary mast lines.

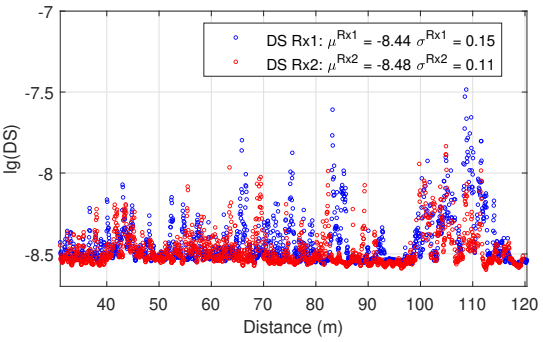

Fig. 9. PL and interval technique for the first Rx.

Then, the logarithmic value of the RMS delay spread is calculated. The mean value for all the measurements is retained, and the results are presented in Tab. V. It can be noted that there is no significant difference in RMS delay spread between antennas with vertical and horizontal polarization. The author in [6] obtained a result of -7.7 for the log RMS delay spread, which is higher than our result, implying a longer RMS delay spread. This result can be explained by the fact that the 60 GHz radio propagation channel is sparser than the one at lower frequencies. Indeed, in [11], the authors present results obtained from Vehicle-to-Vehicle measurements at different mmWave frequencies (30 and 60 GHz) and conclude that the channel is sparser at higher frequencies, as illustrated in this case.

V. CONCLUSION

This paper presents statistical parameters obtained from measurements conducted in a railway environment. The CS used for this campaign is introduced, featuring a 180 MHz available bandwidth to measure the radio propagation channel at 60 GHz. The available environment for measurement is then presented, divided into three different tracks, each used for different scenarios. In the scope of this paper, only the middle track is used for the platooning scenario. In this scenario, the Rx and Tx are placed 80 cm above the ground, which is approximately the height of the coupling mechanism on the train, and are aligned due to the straight railway. From these measurements, statistical parameters such as the PL, the Rice parameters for small-scale fading, and the RMS delay spread are presented. The results show that the radio propagation channel is sparser compared to other millimeter-wave frequencies. Additionally, the propagation losses are higher. This paper also provides, for the first time, parameter fitting for the small-scale fading Rice distribution, divided into the K-Factor and Ω.

ACKNOWLEDGMENT

This work was performed under the mmW4Rail research project financed by the French Research Agency (ANR) under Grant ANR-20-CE22-0011.

REFERENCES

[1] G. Li, B. Ai, K. Guan, R. He, Z. Zhong, B. Hui, and J. Kim, "Channel Characterization for Mobile Hotspot Network in Subway Tunnels at 30 GHz Band," in *2016 IEEE 83rd Vehicular Technology Conference (VTC Spring)*. Nanjing, China: IEEE, May 2016, pp. 1–5. [Online]. Available: http://ieeexplore.ieee.org/document/7504155/

[2] S.-W. Choi, H.-S. Chung, D.-S. Cho, S.-N. Choi, H.-J. Oh, I. Kim, D.-H. Kim, and J.-M. Ahn, "Performance Evaluation of Millimeter-Wave-Based Communication System in Tunnels," in *2015 IEEE Globecom Workshops (GC Wkshps)*. San Diego, CA, USA: IEEE, Dec. 2015, pp. 1–5. [Online]. Available: http://ieeexplore.ieee.org/document/7414003/

[3] S. Choi, H. Chung, J. Kim, J. Ahn, and I. Kim, "Mobile Hotspot Network System for High-Speed Railway Communications Using Millimeter Waves," *ETRI Journal*, vol. 38, no. 6, pp. 1052–1063, Dec. 2016. [Online]. Available: http://doi.wiley.com/10.4218/etrij.16.2716.0018

[4] G. Noh, J. Kim, H. S. Chung, B. Hui, Y.-M. Choi, and I. Kim, "mmWave-Based Mobile Backhaul Transceiver for High Speed Train Communication Systems," in *2017 IEEE Globecom Workshops (GC Wkshps)*. Singapore: IEEE, Dec. 2017, pp. 1–5. [Online]. Available: http://ieeexplore.ieee.org/document/8269215/

[5] J. Kim, M. Schmieder, M. Peter, H. Chung, S.-W. Choi, I. Kim, and Y. Han, "A Comprehensive Study on mmWave-Based Mobile Hotspot Network System for High-Speed Train Communications," *IEEE Transactions on Vehicular Technology*, vol. 68, no. 3, pp. 2087–2101, Mar. 2019. [Online]. Available: https://ieeexplore.ieee.org/document/8438925/

[6] M. Schmieder, M. Peter, R. Askar, I. Komsic, and W. Keusgen, "Measurement and Characterization of 28 GHz High-Speed Train Backhaul Channels in Rural Propagation Scenarios," in *12th European Conference on Antennas and Propagation (EuCAP 2018)*. London, UK: Institution of Engineering and Technology, 2018, pp. 363 (5 pp.)–363 (5 pp.). [Online]. Available: https://digital-library.theiet.org/content/conferences/10.1049/cp.2018.0722

[7] M. Soliman, P. Unterhuber, S. Sand, E. Staudinger, J. Shamshoom, C. Schindler, and A. Dekorsy, "Dynamic Train-to-Train Propagation Measurements in the Millimeter Wave Band - Campaign and First Results," p. 5, 2019.

[8] N. Attwood, F. Gallee, P. Pajusco, and M. Berbineau, "mmWave Channel Sounding for Vehicular Communications," in *2024 18th European Conference on Antennas and Propagation (EuCAP)*. Glasgow, United Kingdom: IEEE, Mar. 2024, pp. 1–5. [Online]. Available: https://ieeexplore.ieee.org/document/10501071/

[9] "Ettus Research - The leader in Software Defined Radio (SDR) | Ettus Research, a National Instruments Brand | The leader in Software Defined Radio (SDR)." [Online]. Available: https://www.ettus.com/

[10] MERCE, "WF on evaluation assumptions for high speed train scenario: Macro + relay at 30GHz."

[11] D. Dupleich, R. Müller, S. Skoblikov, C. Schneider, M. Boban, Jian Luo, G. Del Galdo, and R. Thomä, "Multi-band Spatio-Temporal Characterization of a V2V Environment Under Blockage," in *12th European Conference on Antennas and Propagation (EuCAP 2018)*. London, UK: Institution of Engineering and Technology, 2018, pp. 366 (5 pp.)–366 (5 pp.). [Online]. Available: https://digital-library.theiet.org/content/conferences/10.1049/cp.2018.0725